Design and Optimization of a Slot-PM-assisted Doubly-salient Machine Based on Saturation Assuaging*

Yuan Mao[1*], *Shuangxia Niu*[1] *and Qingsong Wang*[2]

(1. Department of Electrical Engineering, The Hong Kong Polytechnic University, Hong Kong 999077, China;
2. Department of Electrical Engineering, École de Technologie Supérieure, Montreal H3C 1K3, Canada)

Abstract: In this study, a novel slot PM-assisted doubly-salient machine (SPMA-DSM) is proposed based on saturation assuaging. In this machine, DC current is adopted as the excitation source. The permanent magnets assembled in slots are used to realize saturation assuaging, which can offer higher torque density and improved overload capability. Additionally, the torque density can be extended to wider scale before saturation. Multi-objective optimization based on differential evolution (DE) coupled with finite element method (FEM) is conducted to further improve the performance of the proposed machine. When compared to traditional flux-controllable machine, the PMAHEM exhibits the merits of: ① higher torque density per PM volume, ② lower torque ripple, and ③ wider flux controllable range. The simulation results indicate that the electromagnetic torque increases by more than 20% after the saturation assuaging design and optimization.

Keywords: Doubly-salient machine, finite element method, multi-objective optimization, saturation assuaging

1 Introduction

Nowadays, flux controllable machines have attracted significant attention for application in electric vehicles (EVs). Flux regulation can be realized mainly via wound field machines (WFMs), permanent magnetic machines (PMMs), and hybrid-excited machines (HEMs). The introduction of field winding in WFMs can aid in regulating the magnetic field and output capability based on operating conditions. Hence, this is beneficial for the electric vehicles with wide range of speed requirements [1]. However, WFMs suffer from problems such as lower torque density, higher copper loss, and lower efficiency [2]. In PMMs, PM is adopted as the excitation source wherein PM can exhibit higher torque density and higher efficiency. However, flux-regulation is still a problem in PMMs in certain applications [3-5]. In HEMs, field excitation and PM excitation are adopted, and they can exhibit good flux regulation capability without sacrificing the torque density to a certain extent [6-8]. However, there still exist certain challenging issues in HEMs [9-10]. One of the issues involves the saturation effect in ferrite core due to DC field current [11]. Another issue pertains to the instability of the price of rare earth PM materials [12]. Therefore, it is essential to conserve PM volume during the manufacturing of flux controllable machines.

In this study, an improved structure of a doubly-salient machine (DSM), which adopts PM segments in the slots notch to realize saturation assuaging, is proposed to solve the issues. This design is termed as slot-PM-assisted doubly-salient machine (SPMA-DSM). SPMA-DSMs exhibit higher torque density and wider torque range when compared with traditional WFMs. Furthermore, when compared with traditional HEMs, SPMA-DSMs exhibit advantages in terms of higher torque density per PM volume. A large volume of studies have been performed to investigate the structure of SPMA-DSMs. In Ref. [13], DC coils were directly

Manuscript received April 19, 2021; revised June 12, 2021; accepted July 6, 2021. Date of publication September 30, 2021; date of current version August 6, 2021.
* Corresponding Auther, E-mail: yuan.my.mao@connect.polyu.hk
* Supported by the National Natural Science Foundation of China under Project 52077187 and in part by the Research Grant Council of the Hong Kong Government under Project PolyU 152143/18E and PolyU 152109/20E.
Digital Object Identifier: 10.23919/CJEE.2021.000026

introduced wherein the field winding and armature winding share the same stator slots. However, this design can suffer from low utilization of slot space. This in turn leads to unsound torque density performance. In this study, we aim to remedy this problem by constructing a double slot structure that provides better torque performance.

To further improve the torque density and reduce the torque ripple of the proposed SPMA-DSM, multi-objective optimization, based on differential evolution (DE) coupled with finite element method (FEM), is conducted [14-16]. This paper is organized as follows: structure and operating principle of the SPMA-DSM are described in Section 2, performance analysis and comparison studies are presented in Section 3, and machine design and optimization method are discussed in Section 4. Conclusions are drawn in Section 5.

2 Machine structure and operating principles

The configuration of the proposed doubly salient machine is shown in Fig. 1. Typically, there are three common topologies in the machine stator design: the partitioned stator design, which has two air gaps and can lead to unevenness in manufacturing; the single slot structure, which potentially does not fully utilize the stator space; and the double slots structure, which is employed in this study and can separate the dc excitation and ac armature windings. As shown in Fig. 1, the excitation winding slot and armature winding slot are arranged in the inner stator. The DC coils can magnetize the neighboring ferrite salient teeth in opposite directions, which leads to identical flux distribution as consequent PM poles and provides biased flux in the machine. The rotor structure without PMs is very simple and robust. Hence, it is highly suitable for application in EVs. This machine exhibits a double salient structure with 24 slots and 26 rotor poles. The PM segments are embedded in the armature winding slot notch. The magnetization directions of all the PM segments are in tangential directions, which are denoted with arrows in Fig. 1. The main design parameters of the proposed SPMA-DSM are shown in Tab. 1.

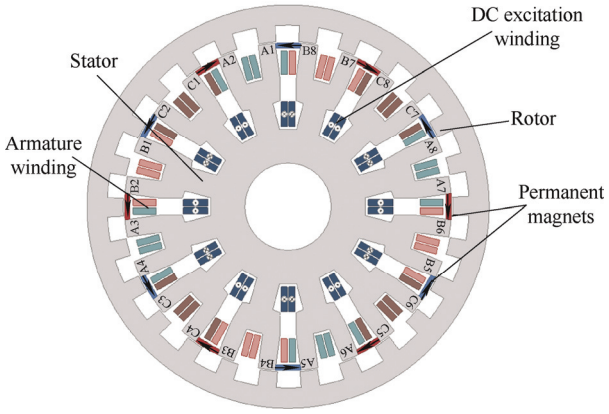

Fig. 1 Configuration of the SPMA-DSM

Tab. 1 Machine parameters

Parameter	Value
Machine outer diameter D/mm	140
Shaft radius R_{shaft}/mm	15
Axial length l_g/mm	100
Air gap length l_{ag}/mm	0.5
Rotor poles N_r	22
Number of inner slots Z_i	12
Number of outer slots Z_o	24
Number of PM pole pairs P_{MS}	6
Number of armature winding conductors N_c	30
Number of field winding conductors N_d	30
Rated speed n/(r/min)	300
Magnetic remanence M_r/T	1.2
Maximum current density ρ/(A/mm^2)	6
Copper space factor Sc(%)	70
Rated field current I_d/A	6
Rated ac current I_a/A	5

The operating principle of the proposed SPMA-DSM can be derived from the "magnetic gear effect" [7]. If the pole pair number (PPN) of slot teeth and rotor pole number are assumed as N_s and N_r, respectively, then the PPN of harmonics after modulation can be expressed as follows

$$\begin{cases} P_{m,k} = \left| mN_s + kN_r \right| \\ m = 1,3,5,7,\cdots \qquad k = 0,\pm1,\pm2,\cdots \end{cases} \tag{1}$$

The corresponding rotational speed of each harmonics is as follows

$$\omega_{m,k} = \frac{kN_r}{mN_s + kN_r}\omega_r \tag{2}$$

where ω_r denotes the angular velocity of the rotor. When the machine operates in brushless AC (BLAC)

mode, the electromagnetic torque equations can be expressed as follows [17]

$$T=\frac{3}{2}N_r\left[\psi_{PM}I_q+\left(L_d-L_q\right)I_dI_q\right] \tag{3}$$

where ψ_{PM} denotes the PM flux linkage, I_d and I_q denote the currents of d- and q-axes, respectively, and L_d and L_q denote the inductance values of d- and q-axes, respectively.

Specifically, $P_{m,k}$ in Eq. (1) illustrates the harmonics order composition after flux modulation. Furthermore, it can be deduced that there are numerous harmonics emerge as the exciter with single pole pair modulated by a specific rotor. For the SPMA-DSM proposed in this study, the conditions can become more complex. This is due to the fact that the field excitation exciter of PMAHEM does not appear as standard consequent PM poles. It is well known that exciter harmonics with the same PPN and rotational speed as those of the armature exciter can interact mutually and produce electromagnetic torque. With respect to the generator mode, the back electromotive force (EMF) can be realized. Furthermore, the pole pair number of armature exciter can be determined based on the finite element method (FEA) of airgap flux density.

The rotor and salient teeth of the slot contribute to the flux-modulation effect. After flux modulation, the air gap PM harmonics with the same PPN and rotation speed as those excited by the armature field interact with each other to generate torque. The feasible slot/rotor pole combination can be formulated as follows [18]

$$\begin{cases} N_s=2q\bullet j & j=1,2,3,\cdots \\ N_r=N_s\pm 2k & k=1,2,3,\cdots \end{cases} \tag{4}$$

where q denotes the phase number. The combinations with odd rotor pole pairs are not used given the influence of unbalanced magnetic pull. In this study, the stator teeth number was selected as 24, and the rotor PPN was selected as 26 to realize relatively higher pole ratio and torque density.

3 Comparative study

To illustrate the advantageous features of the proposed SPMA-DSM, the wound field model (Fig. 2a) and traditional PM-assisted model with 24-DC slots (Fig. 2b) are extracted for comparison. The topology dimensions of all the models are optimized in the maximum output torque.

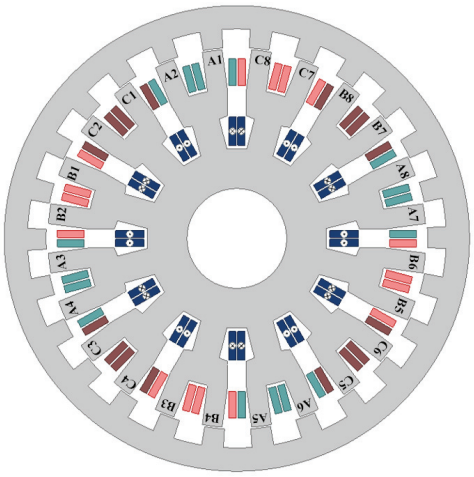

(a) Wound field model

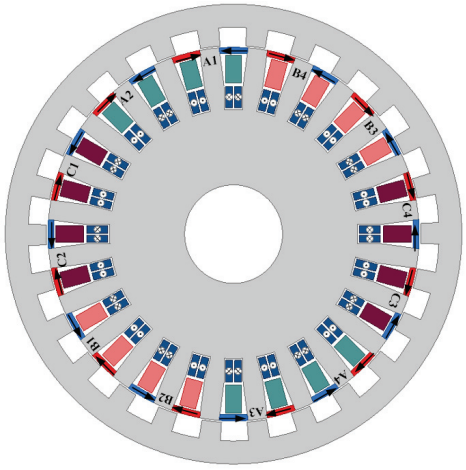

(b) Traditional model

Fig. 2 Topologies of comparative models

3.1 Topology and flux path analysis

Without PM segments, the proposed SPMA-DSM operates similarly to a wound field machine. As shown in Fig. 3a, flux linkages are generated by DC coils only in the wound field model. The effective flux linkages for each module starts from one stator tooth, subsequently enters the aligned rotor poles, and finally returns back from the adjacent stator tooth. By introducing the PM segments, another flux linkage is excited. As depicted in Fig. 3b, the PM flux linkage (labeled by light dash line) emerges in the opposite direction in the stator yoke. Moreover, the PM excited

flux linkage and DC filed excited flux linkage have the same directions in the rotor air gap. This implies that the introduced slot PMs can extend the magnetic saturation point in the proposed PMAHEM, and thus they lead to a good relieving DC-saturation characteristic. A traditional PM- assisted model has 24 DC slots, where the number of PM segments are also doubled. The flux path of this type of machine is shown in Fig. 3c.

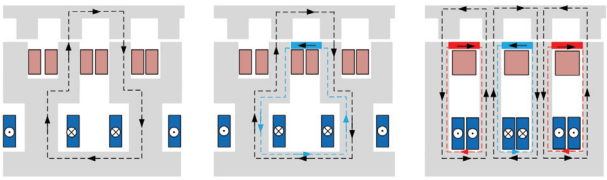

(a) Wound field model (b) Proposed model (c) Traditional model

Fig. 3 Flux path of the machine

3.2 Winding distribution

To realize higher winding factor, winding distribution method based on coil flux linkage analysis is discussed in this section. Coil flux linkages of each type of models are tested under no load conditions. The proposed model and wound field model are designed with double-layer coils, which are sorted into three phases as shown in Fig. 1 and Fig. 2a respectively. The traditional model is devised with single-layer coils which are sorted into three phases as shown in Fig. 2b.

The coil flux linkages are denoted in Fig. 4. It is important to note that the coils that are labeled together and separated by a comma have the same phase and amplitude (e.g., A1, A5). Furthermore, coils with the same initial phase can be arranged into one phase to realize relatively high winding factor.

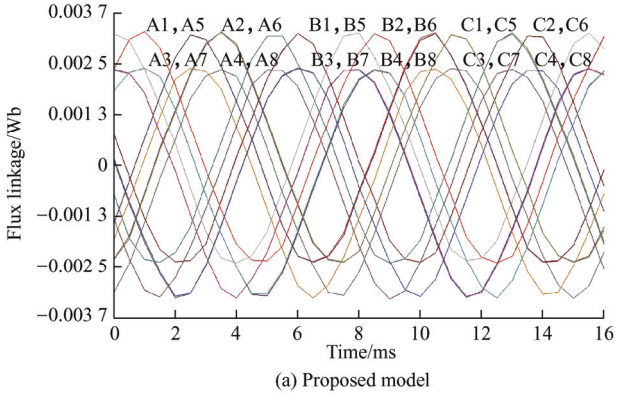

(a) Proposed model

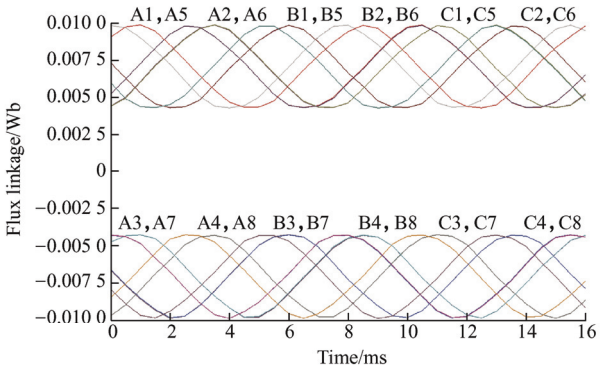

(b) Wound field model

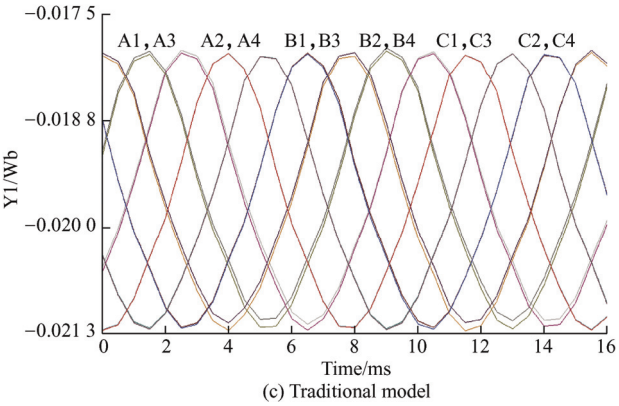

(c) Traditional model

Fig. 4 Coil flux linkage and winding arrangement of the model

3.3 Flux line distribution

To verify the feasibility of the PM-assisted structure, flux line distribution is conducted by using the finite element method (FEM) under rated DC current with no load condition. Furthermore, for comparison, flux line distribution of the wound field model and traditional model are calculated. Fig. 5 shows that additional flux lines are excited by the PM segments in the proposed PM-assisted structure and traditional structure. However, there are fewer flux lines in traditional model that go through the rotor air gap when compared those in the traditional model. This in turn can lead to unsatisfactory torque performance.

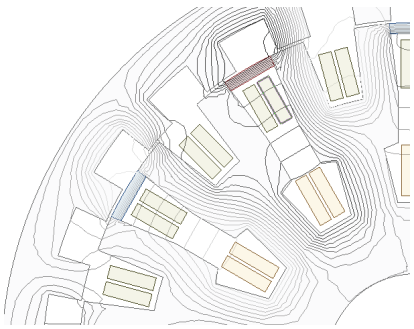

(a) Proposed model

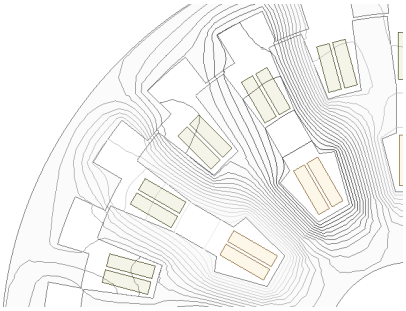

(b) Wound field model

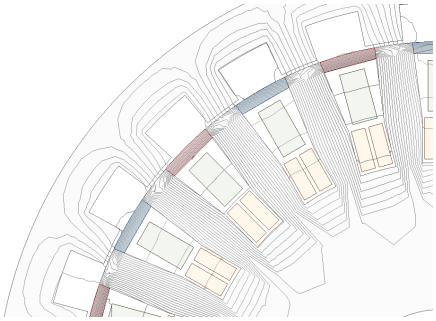

(c) Traditional model

Fig. 5 Flux line distribution using FEM under rated DC current in no-load condition of the model

3.4 Back EMF and torque performance

In the back EMF and torque test, the three models are implemented at the same rated speed and electric load. Thus, the product of field current and conductor number is identical. Fig. 6 shows the no load back EMF waveform of three models under the rated field current. Hence, the back EMF amplitude of the 24-DC slots structure is lower than that of the 12-DC slots structure. The PM-assisted structure of 12-DC slots model does not affect the back EMF in the rated condition.

Furthermore, increases in the load current from 2 A to 20 A in steps of 2 A can theoretically increase output torque. However, given the saturation effect of flux density, torque does not increase further after the current reaches a certain point. Fig. 7 shows the torque versus load current waveform of each model. It is observed that traditional model exhibits the lowest torque in the tested scale from 0-14 A. However, it exceeds the wound field model after 16 A. The proposed SPMA-DSM exhibits the highest torque in the entire tested scale. The traditional and proposed PM assisted machine exhibit higher anti-saturation performance than the wound field model. Signs of saturation are absent in the tested scale of PM-assisted structure, while the saturation point for wound field model is approximately 12 A.

Performances related to torque, torque ripple, total slot area, copper loss, core loss, and efficiency are tested via FEM. The detailed results are listed in Tab. 2. The results indicate that the proposed model exhibits the highest torque production and lowest torque ripple. The wound field model displays larger slot area, and thus it exhibits the lowest copper loss and highest efficiency. However, this can lead to a loss of significant amount of torque without PM excitation. Furthermore, the traditional model with 24-DC slots structure exhibits limitation in terms of the slot area, thereby resulting in low torque and efficiency performance.

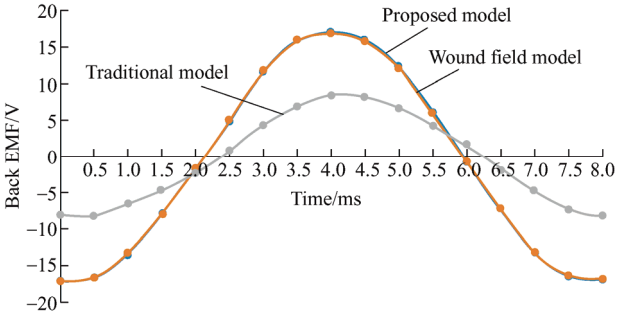

Fig. 6 Back EMF waveforms of each model

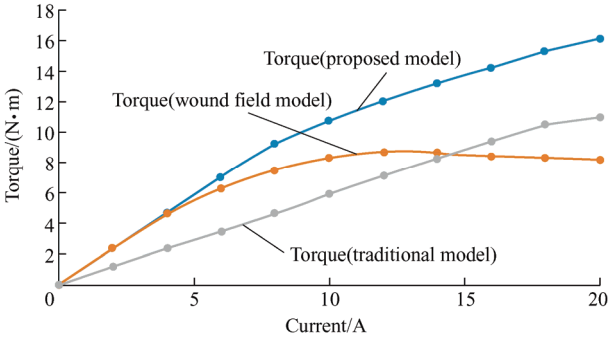

Fig. 7 Torque versus DC current waveforms of each model

Tab. 2 Machine performance of the three models under rated conditions

	Proposed model	Wound field model	Traditional model
Torque/(N • m)	7.0	6.1	3.5
Torque ripple/(N • m)	0.8	1.3	1.6
Total slot area/mm^2	3 493	3 685	2 777
Copper loss/W	13.5	8.5	22.5
Core loss/W	7.9	7.1	12.1
Efficiency(%)	91.9	92.4	76.5

4 Optimization

In the study, the dimension parameters shown in Fig. 8 are optimized using the multi-objective DE coupled with FEM. The objective of the optimization is to realize relatively higher torque and lower torque ripple.

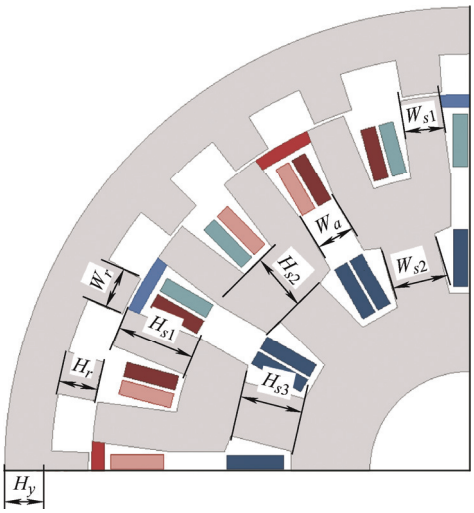

Fig. 8 Dimension parameters of the proposed PMAHEM

Multi-objective optimization differs from traditional single-objective optimization and typically includes a set of solutions that satisfy a predetermined definition for an optimum. A dominant method of defining the optimal solution sets corresponds to Pareto optimality that indicates a solution is Pareto optimal if there is no other point that improves at least one objective function [19-21]. The weighted aggregation method is a common approach in multi-objective optimization and involves congregating several normalized objectives as one multi-objective function with weighting factors [22]. This method is adopted in the study. The objective function is expressed as follows

$$\max z(x) = \omega_1 \frac{T}{T^*} - \omega_2 \frac{T_r}{T_r^*} \tag{5}$$

where x denotes the set of dimension parameters; ω_1 and ω_2 denote weighting factors which should satisfy $\omega_1+\omega_2=1$; T and T_r denote torque and torque ripple, respectively, T^* and T_r^* denote base torque and torque ripple under the original dimension parameter value. Individuals of $\boldsymbol{x}$ should be evaluated between the constraints shown in Tab. 3. It should be noted that the main dimension parameters, such as outer diameter, shaft radius, axial length, and air gap length, listed in Tab. 1, should be maintained as constant. Additionally, the current density should not exceed the rated value. The constraint conditions can be verified after the individuals are generated [23].

Tab. 3 Original and optimized dimension parameters

Dimension parameters	Lower bound	Upper bound
H_r/mm	4	8
H_{s1}/mm	6	14
H_{s2}/mm	6	14
H_{s3}/mm	6	14
H_y/mm	2	8
W_{s1}/mm	2	8
W_{s2}/mm	8	16
W_a/mm	2	8
W_r/mm	2	8

The convergence condition of the optimization is expressed as follows

$$\left|z_i(\boldsymbol{x}) - z_{i-1}(\boldsymbol{x})\right| \leqslant \varepsilon \quad i = 1,2,\cdots,G \tag{6}$$

where $z_i(\boldsymbol{x})$ denotes best solution of the objective function in i^{th} generation, and G denotes the maximum generation number. The optimization flow chart is presented in Fig. 9. The optimization is processed with the following considerations: a population corresponding to 60 elements and maximum generation number corresponding to 30. It should be noted that the main control variables of *DE* correspond to F and CR [24]. With respect to parameter F, 0.5 typically corresponds to a good initial choice, and the normal initial setting of CR is 0.1 [24]. Based on the convergence rate and accuracy, the control variable F and CR are set as 0.7 and 0.1 respectively [25]. Additionally, the weighting factor of torque and torque ripple are set as 0.5. The dimension parameters before and after optimization are listed in Tab. 4.

The original average torque is 5.1 N • m, while the optimized average torque is 7.0 N • m. The torque ripple before optimization is approximately 1.6 N • m while it corresponds to 0.8 N • m after optimization. A multi-objective optimization combining FEA and DE increases the average torque of HEBFM by 37.1%, and the torque ripple decreases by 50.0%.

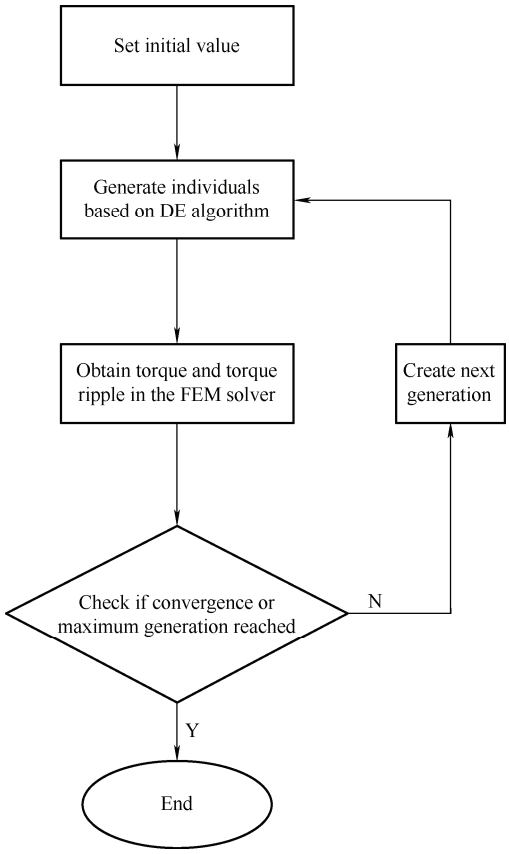

Fig. 9 Flowchart of the optimization process

Tab. 4 Original and optimized dimension parameters

Dimension parameters	Original value	Optimized value
H_r/mm	6.0	5.6
H_{s1}/mm	10.0	11.9
H_{s2}/mm	10.0	9.0
H_{s3}/mm	10.0	9.3
H_y/mm	5.0	5.9
W_{s1}/mm	5.0	6.0
W_{s2}/mm	10.0	8.3
W_a/mm	5.0	5.7
W_r/mm	5.0	6.0

5 Conclusions

In this study, an improved design of a hybrid-excited machine is proposed to solve saturation issues. Specifically, PM segments with tangential magnetization directions are introduced to counteract original flux linkage produced by excitation current. When compared with the wound field model and traditional 24-DC slots structure model, the proposed model exhibits better saturation assuaging performance. A multi-objective optimization is employed. It increases the torque by 37.1% and decreases torque ripple by 50%. The FEM test results of flux density, back EMF, and torque density effectively verify the feasibility of the design.

References

[1] Z Q Zhu, S Cai. Hybrid excited permanent magnet machines for electric and hybrid electric vehicles. *CES Transaction On Electrical Machines and Systems*, 2019, 3(3): 233-247.

[2] H Polinder, J A Ferreira, B B Jensen, et al. Trends in wind turbine generator systems. *IEEE Journal of Emerging and Selected Topics in Power Electronics*, 2013, 1(3): 174-185.

[3] M Cheng, W Hua, J Zhang, et al. Overview of stator-permanent magnet brushless machines. *IEEE Trans. Ind. Electron.*, 2011, 58(11): 5087-5101.

[4] S Hwang, J Sim, J Hong, et al. Torque improvement of wound field synchronous motor for electric vehicle by PM-assist. *IEEE Trans. Ind. Appl*., 2018, 54(4): 3252-3259.

[5] R Owen, Z Q Zhu, J B Wang, et al. Review of variable-flux permanent magnet machines. *in Proc. 2011 International Conference on Electrical Machines and Systems*, Beijing, 2011: 1-6.

[6] Q Wang, S Niu, X Luo. A novel hybrid dual-PM machine excited by AC with DC bias for electric vehicle propulsion. *IEEE Trans. Ind. Electron*., 2017, 64(9): 6908-6919.

[7] X Luo, T A Lipo. A synchronous/permanent magnet hybrid AC machine. *IEEE Trans. Energy Convers*., 2000, 15(2): 203-210.

[8] T Kosaka, M Sridharbabu, M Yamamoto, et al. Design studies on hybrid excitation motor for main spindle drive in machine tools. *IEEE Trans. Ind. Electron*., 2010, 57(11): 3807-3813.

[9] W Ullah, F Khan, M Umair. Optimal rotor poles and structure for design of consequent pole permanent magnet flux switching machine. *Chinese Journal of Electrical Engineering*, 2021, 7(1): 118-127.

[10] J Zheng, W Zhao, J Ji, et al. Sleeve design of permanent-magnet machine for low rotor losses. *Chinese Journal of Electrical Engineering*, 2020, 6(4): 86-96.

[11] Q S Wang, S Niu. Overview of flux-controllable machines: Electrically excited machines, hybrid excited machines and memory machines. *Renewable Sustainable Energy Rev*., 2017, 68: 475-491.

[12] X Zhao, S Niu. Design and optimization of a novel slot-PM-assisted variable flux reluctance generator for

hybrid electric vehicles. *IEEE Trans. Energy Convers*., 2018, 33(4): 2102-2111.

[13] X Zhao, S Niu, W Fu. A new modular relieving-dc-saturation vernier reluctance machine excited by zero-sequence current for electric vehicle. *IEEE Trans. Magn*., 2019, 55(7): 1-5.

[14] K Deb, A Pratap, S Agarwal, et al. A fast and elitist multiobjective genetic algorithm: NSGA-II. *IEEE Transactions on Evolutionary Computation*, 2002, 6(2): 182-197.

[15] Y Mao, S Niu, Y Yang. Differential evolution-based multi objective optimization of the electrical continuously variable transmission system. *IEEE. Trans. Ind. Electron*., 2018, 65(3): 2080-2089.

[16] A Ibrahim, M B Shafik, M Ding, et al. PV maximum power-point tracking using modified particle swarm optimization under partial shading conditions. *Chinese Journal of Electrical Engineering*, 2020, 6(4): 106-121.

[17] R L Owen, Z Q Zhu, G W Jewell. Hybrid-excited flux-switching permanent-magnet machines with iron flux bridges. *IEEE Trans. Magn*., 2010, 46(6): 1726-1729.

[18] X Zhao, S Niu, W N Fu. Design of a novel parallel-hybrid-excited dual-PM machine based on armature harmonics diversity for electric vehicle propulsion. *IEEE Trans. Ind. Elec*., 2019, 66(6): 4209-4219.

[19] D Li, Ronghai Qu, Jian Li. Topologies and analysis of flux-modulation machines. *2015 IEEE Energy Conversion Congress and Exposition* (*ECCE*), Montreal, QC, Canada, Sept. 2015.

[20] K Atallah, D Howe. A novel high-performance magnetic gear. *IEEE Trans. Magn*., 2001, 37(4): 2844-2846.

[21] C C Hwang, C M Chang, C T Liu. A fuzzy-based Taguchi method for multi-objective design of PM motors. *IEEE Trans. Magn.*, 2013, 49(5): 2153-2156.

[22] P Jiang, F Liu, J Wang, et al. Cuckoo search-designated fractal interpolation functions with winner combination for estimating missing values in time series. *Appl. Math. Model.*, 2016, 40(23): 9692-9718.

[23] M Ashabani, Y Abdel-Rady, I Mohamed, et al. Optimum design of tubular permanent-magnet motors for thrust characteristics improvement by combined Taguchi-neural network approach. *IEEE Trans. Magn*., 2010, 46(12): 4092-4100.

[24] R Storn, K Price. Differential evolution: A simple and efficient heuristic for global optimization over continuous spaces. *Journal of Global Optimization*, 1997, 11: 341-359.

[25] Y Mao, S Niu. Topology exploration and analysis of a novel winding factor modulation based hybrid-excited biased-flux machine. *IEEE Journal of Emerging and Selected Topics in Power Electronics*. Apr. 2021. DOI: 10.1109/JESTPE.2021.3071 923.

Yuan Mao received the B.Sc. degree in Electrical Engineering from the School of Electrical Engineering and Automation, Wuhan University, Wuhan, China, in 2012, and the M.Sc. degree in Electrical and Electronics Engineering from the Department of Electrical and Electronics Engineering, The University of Hong Kong, Hong Kong, China, in 2014. She is currently working toward the Ph.D. degree in the Department of Electrical Engineering, The Hong Kong Polytechnic University, Kowloon, Hong Kong, China.

Her research interests include the design, optimization and control of dual-port and multi-port flux-modulation electrical machines.

Shuangxia Niu (Senior Member, IEEE) received the B.Sc. and M.Sc. degrees in Electrical Engineering from the School of Electrical Engineering and Automation, Tianjin University, Tianjin, China, and the Ph.D. degree in Electrical Engineering from The University of Hong Kong, Hong Kong, China, in 2009. Since 2009, she has been with The Hong Kong Polytechnic University, Hong Kong, China, where she is currently an Associate Professor with the Department of Electrical Engineering. She has authored or co-authored more than 100 articles in leading journals.

Her research interests include the design and control of novel electrical machines and drives, renewable energy conversion systems, and applied electromagnetics.

Qingsong Wang (Member, IEEE**)** received the B.Sc. degree from the College of Automotive Engineering, Jilin University, Changchun, China, in 2012, the M.Sc. degree from the School of Automotive Studies, Tongji University, Shanghai, China, in 2015, and the Ph.D. degree from the Department of Electrical Engineering, The Hong Kong Polytechnic University, Hong Kong, China, in 2018. From 2018 to 2019, he was a Postdoctoral Research Fellow with the University of British Columbia, Vancouver, BC, Canada. He is currently an Assistant Professor at Department of Electrical Engineering, École de Technologie Supérieure, Montreal, Quebec, Canada.

His research interests include electrical machines and drives, wireless power transfer systems, EV/HEV propulsion, and renewable energy systems.